On non-Newtonian effects in fluidic shock-absorbers

Cite as: Appl. Phys. Lett. **117**, 153701 (2020); https://doi.org/10.1063/5.0023938
Submitted: 03 August 2020 . Accepted: 29 September 2020 . Published Online: 12 October 2020

L. Goldstein, D. Ilssar and A. D. Gat

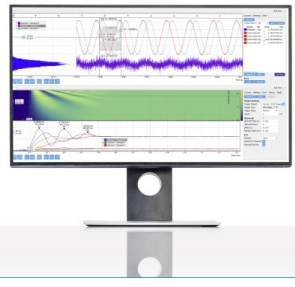

Applied Physics Letters ARTICLE scitation.org/journal/apl

On non-Newtonian effects in fluidic shock-absorbers

Cite as: Appl. Phys. Lett. **117**, 153701 (2020); doi: 10.1063/5.0023938
Submitted: 3 August 2020 · Accepted: 29 September 2020 ·
Published Online: 12 October 2020

L. Goldstein, D. Ilssar, and A. D. Gat[a)]

AFFILIATIONS

Faculty of Mechanical Engineering, Technion-Israel Institute of Technology, Haifa 3200003, Israel

[a)]Author to whom correspondence should be addressed: amirgat@technion.ac.il

ABSTRACT

Shock-absorbers often involve throttling of viscous fluids through small orifices. This gives rise to high rates-of-strain and non-Newtonian behavior even in fluids which are commonly assumed Newtonian, which affects impact mitigation properties. We here derive an asymptotic approximation describing the dynamics of fluidic shock-absorbers while focusing on weak Carreau type non-Newtonian effects and annular geometries. We validate our model by numerical computations and experiments with a medium-sized shock-absorber used to mitigate the impact caused by a free-falling weight. We then leverage the theoretical model to calculate the shock-absorber's optimal geometry and present experimental results of the fabricated optimal configuration, showing good agreement with the theory and nearly optimal impact mitigation properties.

Hydraulic dampers and shock-absorbers exploit the resistance to motion of confined fluids in order to temporally redistribute the momentum of a sudden impact, over a larger time period. The most common method is throttling fluid through an orifice in various constant or spatially varying sizes and shapes, creating a differential pressure across the orifice, which acts as a retarding force. This retarding force modifies and slows the motion of the mass.

Common configurations include squeeze-film dampers, employing the viscous forces exerted by a thin fluidic film trapped between two closely spaced conformal surfaces, exhibiting normal motion.[1–3] This configuration is typically utilized in small-scale devices. In macro-scale systems, passive fluidic shock-absorbers frequently exploit the forces exerted by a lubrication film trapped between adjacent conformal surfaces, undergoing transverse relative motion. Such a configuration can be found in the suspension systems of vehicles,[4,5] as well as in tall buildings, where meter-scale dampers are distributed along them to mitigate vibrations caused by strong winds and earthquakes.[6–8]

This work deals with simplified modeling of shock-absorbers exhibiting non-Newtonian fluidic effects, while focusing on annular configurations such as the one presented in Fig. 1, aiming to predict and optimize their performance. The examined system consists of a shaft and a piston whose radii are r_{shaft} and r_{piston}, moving along a joint axis due to an external impact, and viscous fluid contained between this moving part and a fixed outer cylinder. The volume in which the fluid resides comprises two chambers bounded between the shaft and the cylinder and a narrow gap confined between the piston and the cylinder, whose axial dimension denoted l is the length of the piston. Denoting the radius of the cylinder r_{cylinder}, we define the thickness of the narrow gap by $h = r_{\text{cylinder}} - r_{\text{piston}}$ and require $h \ll r_{\text{cylinder}} - r_{\text{shaft}}$. Thus, the dominant fluidic resistance occurs at this narrow gap, and the pressures in the chambers are considered approximately uniform. Since the lateral dimensions of the gap are significantly larger compared with its thickness $h \ll r_{\text{piston}}$, the annular configuration is modeled by a local Cartesian system. In this system, the vertical coordinate corresponding to the radial direction and whose origin is located at r_{piston} is denoted by y, whereas the axial coordinate is denoted by x. Furthermore, since the gap is considered narrow such that $h/l \ll 1$, the reduced Reynolds number defined by $Re_r = \rho u^* h^2/\mu l$ is small, where ρ, μ, and u^* are the density of the fluid, the dynamic viscosity relating the shear stress to the shear rate, and a characteristic value of the axial flow velocity u. Thus, assuming that the fluid is incompressible, the flow inside the narrow gap is described by the lubrication approximation,[9] nulling the pressure gradients and flow velocities along the thickness of the gap, and given by $\partial p/\partial x = \partial(\mu \partial u/\partial y)/\partial y$ along with $\partial p/\partial y = 0$.

When undergoing significant impacts, hydraulic shock-absorbers commonly exhibit substantial shear and pressure force variations, causing, in many cases, the emergence of non-Newtonian effects.[10,11] We model the deviations from Newtonian behavior by the Generalized Newtonian fluid model derived by Carreau,[12] which is extensively utilized to describe biological flows,[13,14] emulsions,[15,16] and

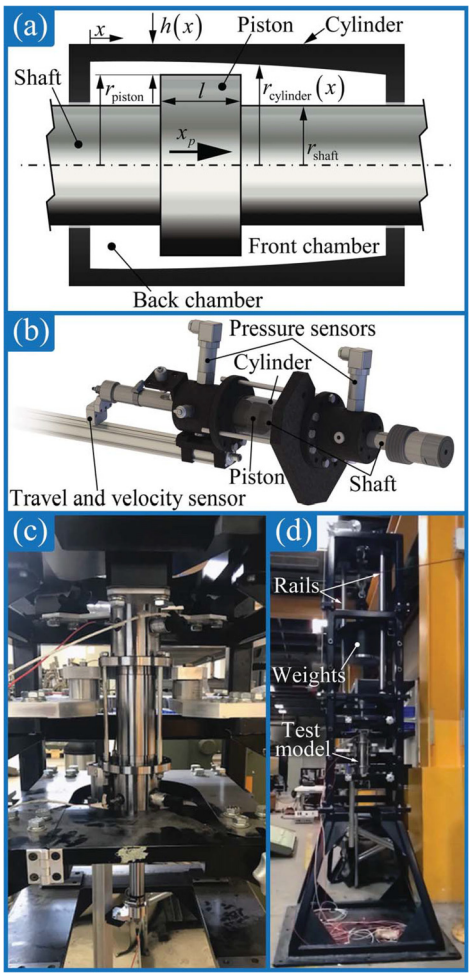

FIG. 1. (a)–(c) A schematic layout, a CAD model, and a photograph of an annular shock-absorber consisting of a shaft and a piston, as well as a cylinder with a customized, axially varying inner radius. (d) A photograph of the entire experimental setup including a free falling weight, which slides along guiding rails from a dictated initial height, and the shock-absorber decelerating the weight's motion.

more. This model enables capturing the Newtonian behavior occurring at low shear rates, as well as shear-thinning effects exhibited in higher rates by silicon oils, which are commonly utilized in viscous dampers.[17–20] The shear-rate dependent viscosity according to the Carreau constitutive model is given by the form $\mu = \mu_0[1 + (\lambda\partial u/\partial y)^2]^{(n-1)/2}$, where μ_0, λ, and n are three empirically determined constants. These represent the zero shear-rate viscosity, a relaxation time constant, and a power-law index corresponding to shear-thinning when $n < 1$. Substituting the viscosity model into the lubrication equation yields the governing equation for the flow within the narrow gap given by

$$\frac{\partial p}{\partial x} = \frac{\partial}{\partial y}\left\{\mu_0\left[1 + \left(\lambda\frac{\partial u}{\partial y}\right)^2\right]^{(n-1)/2}\frac{\partial u}{\partial y}\right\}. \tag{1}$$

This equation is supplemented by the boundary conditions $u(y = 0) = \dot{x}_p$ and $u(y = h) = 0$, where $\dot{x}_p$ is the piston's velocity.

To consider the dynamic behavior of the system, the fluidic problem is combined with the integral momentum balance of the piston given by $m\ddot{x}_p = F_{\text{pressure}} + F_{\text{shear}} + F_{\text{body}}$. Here, in agreement with the experimental rig in Figs. 1(c) and 1(d), m denotes only the mass of the dampened weight, neglecting all other inertial effects. Furthermore, the terms on the right hand side of Eq. (1) are, in order, the force applied due to the pressure difference between the uniform pressure chambers, the shear force exerted by the fluid in the thin gap, and body forces. Order of magnitude analysis using $h \ll r_{\text{cylinder}} - r_{\text{shaft}}$ allows us to further neglect the shear forces applied to the piston, compared with the normal forces acting on its front and back faces. Thus, the integral momentum equation governing $x_p(t)$ is

$$m\ddot{x}_p \approx mg - \pi\left(r_{\text{piston}}^2 - r_{\text{shaft}}^2\right)\Delta p(x_p, \dot{x}_p), \tag{2}$$

where g is the acceleration due to gravity and Δp is the pressure difference between the front and back chambers. Modifying the inner radius of the cylinder as a function of x yields a non-constant gap, enabling us to optimize the system's behavior. Here, the axial variation of the gap is considered mild such that $dh/dx \ll 1$, allowing us to refer to it as spatially constant, e.g., $\approx h(x_p(t))$.

We now wish to find a closed-form solution of Eq. (1), accounting for the behavior of the fluid inside the narrow gap. For this, we normalize it by $U = u/u^*$, $Y = y/h^*$, $X = x/l$, and $P = p/(u^* l\mu_0/(h^*)^2)$, where h^* is a typical thickness of the gap. Furthermore, u^* is the characteristic flow velocity defined as the volumetric flow rate out of the upstream chamber, averaged by the gap's cross section, thus given by $u^* \approx \dot{x}_p[\pi(r^*_{\text{cylinder}})^2 - \pi r^2_{\text{shaft}}]/2\pi r_{\text{piston}} h^*$. The latter leads to the following nondimensional form of Eq. (1): $\partial P/\partial X = \partial\left\{[1 + C_r^2(\partial U/\partial Y)^2]^{(n-1)/2}\partial U/\partial Y\right\}/\partial Y$, where the ratio $C_r = \lambda u^*/h^*$ is the Carreau number,[21,22] which quantifies the deviations from Newtonian behavior. Considering relatively weak non-Newtonian effects, C_r serves as a small parameter. Thus, focusing on the limit of $C_r^2 \ll 1$, we employ the regular asymptotic expansion $u = u_0 + C_r^2 u_1 + O(C_r^4)$, along with the Taylor expansion $(1 + C_r^2 f^2)^m = 1 + mC_r^2 f^2 + O(C_r^4)$. Solving consecutively for the leading and first orders yields the first-order approximation of the axial flow velocity, given in its dimensional form by

$$\begin{aligned} u \approx{}& \frac{y(y-h)}{2}\left[1 + \frac{3(1-n)\lambda^2\dot{x}_p^2}{2h^2}\right]\frac{\Delta p}{\mu_0 l} \\ &- \frac{(1-n)\lambda^2 y(h-y)(h-2y)\dot{x}_p}{4h}\left(\frac{\Delta p}{\mu_0 l}\right)^2 \\ &- \frac{(1-n)\lambda^2 y(h-y)\left(h^2 - 2hy + 2y^2\right)}{16}\left(\frac{\Delta p}{\mu_0 l}\right)^3 \\ &+ \frac{(h-y)\dot{x}_p}{h}, \end{aligned} \tag{3}$$

with errors scaling as $O(C_r^4)$. Integration of this expression over the gap's cross section yields the volumetric flow rate from the front to the back chamber. An additional expression for this flow rate is calculated by the time derivative of the upstream chamber's volume, yielding a kinematic relation in terms of piston's motion. Equating these two

expressions for the volumetric flow rate provides a third order algebraic relation between the pressure difference and the piston's motion. Substituting the physical solution of the latter into Eq. (2) yields the following form of the shock-absorber's equation of motion:

$$m\ddot{x}_p \approx mg - 2\pi h^{-1}\mu_0 l\left(r_{\text{piston}}^2 - r_{\text{shaft}}^2\right)\left[\sqrt{\left(\frac{10\psi}{9}+\frac{5\dot{x}_p^2}{3h^2}\right)^3 + 25h^{-4}\psi^2(h+\Upsilon)^2\dot{x}_p^2} + 5h^{-2}\psi(h+\Upsilon)\dot{x}_p\right]^{-1/3}$$
$$\times\left[\left(\sqrt{\left(\frac{10\psi}{9}+\frac{5\dot{x}_p^2}{3h^2}\right)^3 + 25h^{-4}\psi^2(h+\Upsilon)^2\dot{x}_p^2} + 5h^{-2}\psi(h+\Upsilon)\dot{x}_p\right)^{2/3} - \frac{10\psi}{9} - \frac{5\dot{x}_p^2}{3h^2}\right]. \quad (4)$$

Here, $\Upsilon = (r_{\text{cylinder}}^2 - r_{\text{shaft}}^2)/r_{\text{piston}}$ is a geometric parameter, whereas $\psi = \lambda^{-2}(1-n)^{-1}$ is a fluidic parameter, encapsulating all non-Newtonian effects. Recalling that h is dependent on x_p, Eq. (4) serves as a basis for an inverse problem, enabling us to find the optimal profile of the axially varying gap.

The analytical results (which are presented and discussed later on) were validated numerically by a commercial finite-volume software (Ansys Fluent™), considering laminar flow that behaves according to the Carreau model. The numerical scheme describes the transnational motion of the system as well as the external forces applied on it, while due to the instantaneous change of geometry, an adaptive mesh utilizing 40 000 cells was implemented. Furthermore, the theoretical results were also verified experimentally, utilizing the drop-test setup presented in Figs. 1(c) and 1(d). This experimental setup consists of an annular shock-absorber used to decelerate the motion of a free-falling mass weighting 105 kg, sliding on guiding rails from different initial heights. The shock-absorber shown in Figs. 1(b) and 1(c) comprises a piston whose outer radius and length are 25 mm and 20 mm, attached to a shaft whose radius is equal to 14 mm. These move inside a sealed interchangeable cylinder, filled with silicon oil with the room-temperature density and kinematic viscosity of 970 kg/m^3 and 1000 cSt. The experimental rig is equipped with lifting and quick-release mechanisms, allowing us to elevate the dampened weight to a desired height and to instantly release it. This enables us to change the impact velocity, which can be estimated from energy conservation of a free falling mass. The pressure at the chambers bounding the piston was measured with piezoelectric sensors whose rise times are 1 μs. The sensor used in the lower chamber is 2300V5 by Dytran Instruments, Inc., having a full-scale of 34.5 MPa, whereas the sensor used at the upper chamber is 113B24 by PCB Piezotronics, having a full-scale of 6.9 MPa. The motion of the shaft and piston was measured by the magnetostrictive transducer MAB 400 by WayCon, comprising a static transducer attached to the cylinder and a moving magnet attached to the shaft. This transducer has a full-scale linearity of less than 0.02% for the travel measurements and less than 2% for the velocity measurements. Furthermore, its resolution is less than 0.2 mm, where its minimal measurable velocity is 0.1 m/s. All the data were gathered by a data acquisition system assembled of a National Instruments NI9178 chassis with NI9215, NI9211, and NI9234 modules, connected to the data acquisition software "LabView signal express." The data were sampled at a rate of 20 kHz and stored for later processing.

The first experiment set executed utilized a cylinder with a constant inner radius of 26.2 mm to calibrate the parameters of the non-Newtonian viscosity model. Using this setup, a series of drop experiments were conducted where the mass was released from various heights, yielding different initial impact velocities. The pressure-velocity relations achieved in these experiments were utilized to calibrate the different parameters through the asymptotic relation, which led to Eq. (4). The latter provided the following values: $\lambda = 3\times10^{-5}$, $n = 0.4$.

Figure 2 presents the relation between the pressure difference among the bounding chambers and the Carreau number which is linearly dependent on the piston's velocity, as measured in four drop experiments having initial impact velocities of 1.54, 1.87, 2.8, and 3.16 m/s. These are presented only along the steady period, after the system finished accelerating due to the initial impact, and before the strong deceleration caused when the piston approached its maximal range of motion. Furthermore, the figure also displays the corresponding values achieved numerically from two-dimensional axisymmetric transient finite-volume simulations carried out in Ansys Fluent. The above-mentioned simulations describe the motion of the piston and the resultant flow field, considering the Carreau model with the empirically obtained parameters. For model verification, the pressure-Carreau number relations according to the approximated non-Newtonian model and

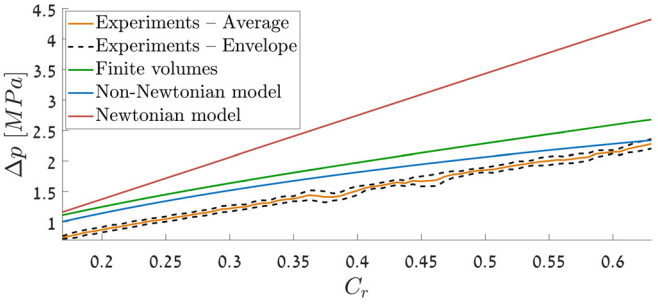

FIG. 2. Experimental, numerically simulated, and analytical results describing the relation between the Carreau number and the pressure difference among the two chambers. The experimental results show the average values alongside their envelope of one standard deviation. Furthermore, the analytical results are computed based on the asymptotic expression that led to Eq. (4) and a Newtonian model that disregard shear-thinning effects.

its Newtonian form where $C_r = 0$ are also presented and compared to the numerical and experimental results. Figure 2 shows that there are significant deviations between the Newtonian model that predicts a linear relation between the velocity and the resisting force, and the Carreau model that considers shear-thinning, thus forecasting lower resistance at higher velocities. This confirms that the non-Newtonian effects are indeed substantial although the examined Carreau numbers are small. Furthermore, there is an overall good agreement between the experimental and theoretical results achieved from the non-Newtonian model. This correlation agrees well even at relatively high Carreau numbers, outside of the expected validity region of the asymptotic approximation. Finally, the good agreement between the model and the numerical results implies that the assumptions made in the asymptotic analysis and the assumption that the flow is fully developed throughout the motion are indeed valid.

To shed light on the overall dynamics of the investigated system, Fig. 3 shows the four dynamic responses achieved in the experiments discussed above, where the initial impact velocities are 1.54, 1.87, 2.8, and 3.16 m/s, and all other parameters are defined above. These are displayed alongside the corresponding theoretical results obtained from our model given by Eq. (4). Figure 3 shows that in all cases, the shock-absorber did not manage to bring the system to rest before the piston reached the flange, sealing the lower part of the cylinder. Nevertheless, the dynamic model shows a very good correlation along the period of steady motion, supporting the validity of the model and its underlying assumptions.

Since the simplified model shows a good correlation with the experimental observations, it was utilized to design an optimal axially varying profile of the cylinder's inner radius, providing superior impact mitigation. Optimal damping is given for constant deceleration, leading to a linearly decreasing velocity given by $\dot{x}_p(t) = \dot{x}_p(0)[1 - \dot{x}_p(0)t/2x_{\text{end}}]$, where $\dot{x}_p(0)$ is the initial velocity and x_{end} is the desired damping range. The wanted constant deceleration was calculated from the derivative of this relation, using a predicted impact velocity of approximately $\dot{x}_p(0) = 3.07$ m/s and a designated damping range of about $x_{\text{end}} = 148.6$ mm, bringing the system to rest with a slight tolerance from the maximal stroke of 160 mm. The latter was followed by computations of the gap, keeping the deceleration constant at every lower velocity, utilizing Eq. (4). Finally, the axial position corresponding to each velocity was computed by integrating the above linear expression, resulting in the axially varying gap presented in Fig. 4 by the solid black curve. Here, the displayed values represent the nominal instantaneous gap, taken at the median axial position of the piston. As seen from this figure, the gap begins at about 1 mm and decreases gradually, slowing down the Carreau number reduction, what according to Fig. 2 increases the resisting forces compared to a uniform profile. This trend proceeds up until a significant drop near the end of the travel, which violates the assumption claiming that the gap can be approximated as instantaneously uniform. Thus, the above-mentioned optimal profile was truncated and was kept at a constant value near the end of the travel; see the dashed curve in Fig. 4.

Figure 4 shows the measured dynamic response achieved in an additional drop test that was conducted using the optimized configuration, where the initial impact velocity was approximately 3.18 m/s. Additionally, this figure shows the corresponding theoretical response obtained by numerically solving Eq. (4). Figure 4 shows very good agreement between the experiments and the theory, where the velocity of the system indeed decreased linearly before the truncation of the profile, and thus the optimized configuration managed to keep the pressure difference constant. Furthermore, it can be seen that after the truncation, the shock-absorber becomes less efficient as the velocity reduction became slower. This non-optimal behavior occurs since after the truncation, the uniform profile does not compensate on the Carreau number reduction, which leads to lower resisting forces. Finally, it should be noted that the theoretical computations were terminated once the piston reached its limit of 160 mm.

To summarize, we have presented an analytical approximation of a high shear-rate non-Newtonian flow within a fluidic shock-absorber, based on the Carreau viscosity model, considering small Carreau numbers. The latter resulted in a simplified model, enabling us to predict the behavior of such a mechanism and to optimize its performance. The suggested model was validated by comparison with finite-volume computations and with data from drop-test experiments, utilizing a simple shock-absorber having a constant gap. The experimental and theoretical results show that even in low Carreau numbers, non-Newtonian effects are significant. Thus, in order to achieve tailored damping rates, it is crucial to consider these effects. Indeed, we have leveraged the proposed model for the design of a shock-absorber with an optimal profile. Comparison between experimental and theoretical results of the optimized configuration showed both excellent agreement and near optimal behavior. The ability to accurately modify the velocity profile of shock-absorbers can be beneficial for diverse

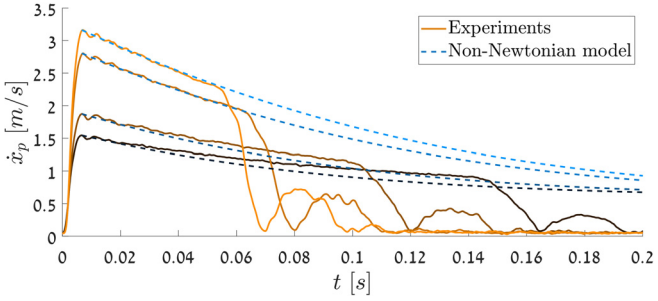

FIG. 3. Comparison between the experimental and theoretical dynamic responses of the system while utilizing a cylinder having a uniform inner profile. These are given in terms of piston's velocity.

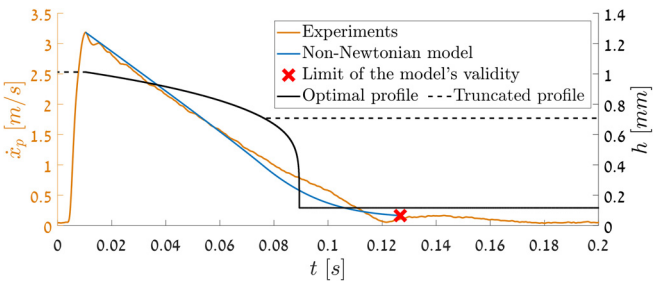

FIG. 4. Comparison between the experimental and theoretical dynamic responses of the optimized system, alongside the instantaneous optimal nominal profile, and its truncated form, which was implemented in practice.

applications including vibration mitigation in vehicles and high-rise buildings.

We thank Dr. Evgeniy Boyko for the discussions regarding this manuscript.

DATA AVAILABILITY

The data that support the findings of this study are available from the corresponding author upon reasonable request.

REFERENCES

[1]W. Griffin, H. H. Richardson, and S. Yamanami, "A study of fluid squeeze-film damping," J. Basic Eng. **88**, 451–456 (1966).
[2]M. Bao and H. Yang, "Squeeze film air damping in MEMS," Sens. Actuators, A **136**, 3–27 (2007).
[3]J. J. Blech, "On isothermal squeeze films," J. Lubr. Technol. **105**, 615–620 (1983).
[4]J. Łuczko and U. Ferdek, "Nonlinear dynamics of a vehicle with a displacement-sensitive mono-tube shock absorber," Nonlinear Dyn. **100**, 185–202 (2020).
[5]C.-T. Lee and B.-Y. Moon, "Simulation and experimental validation of vehicle dynamic characteristics for displacement-sensitive shock absorber using fluid-flow modelling," Mech. Syst. Signal Process. **20**, 373–388 (2006).
[6]J. Whittle, M. Williams, T. Karavasilis, and A. Blakeborough, "A comparison of viscous damper placement methods for improving seismic building design," J. Earthquake Eng. **16**, 540–560 (2012).
[7]H. C. Huang, "Efficiency of the motion amplification device with viscous dampers and its application in high-rise buildings," Earthquake Eng. Eng. Vib. **8**, 521–536 (2009).
[8]R. J. Mcnamara and D. P. Taylor, "Fluid viscous dampers for high-rise buildings," Struct. Des. Tall Spec. Buildings **12**, 145–154 (2003).
[9]L. G. Leal, *Advanced Transport Phenomena: Fluid Mechanics and Convective Transport Processes* (Cambridge University Press, 2007), Vol. 7.
[10]B. J. Hamrock, S. R. Schmid, and B. O. Jacobson, *Fundamentals of Fluid Film Lubrication* (CRC Press, 2004).
[11]H. A. Barnes, J. F. Hutton, and K. Walters, *An Introduction to Rheology* (Elsevier, 1989), Vol. 3.
[12]P. J. Carreau, "Rheological equations from molecular network theories," Trans. Soc. Rheol. **16**, 99–127 (1972).
[13]J. R. Vélez-Cordero and E. Lauga, "Waving transport and propulsion in a generalized Newtonian fluid," J. Non-Newtonian Fluid Mech. **199**, 37–50 (2013).
[14]E. E. Riley and E. Lauga, "Empirical resistive-force theory for slender biological filaments in shear-thinning fluids," Phys. Rev. E **95**, 062416 (2017).
[15]M. Dolz, M. Hernández, J. Delegido, M. Alfaro, and J. Muñoz, "Influence of xanthan gum and locust bean gum upon flow and thixotropic behaviour of food emulsions containing modified starch," J. Food Eng. **81**, 179–186 (2007).
[16]J. E. Moros, J. M. Franco, and C. Gallegos, "Rheology of spray-dried egg yolk-stabilized emulsions," Int. J. Food Sci. Technol. **37**, 297–307 (2002).
[17]C.-Y. Hou, "Fluid dynamics and behavior of nonlinear viscous fluid dampers," J. Struct. Eng. **134**, 56–63 (2008).
[18]J. Uddin, J. O. Marston, and S. T. Thoroddsen, "Squeeze flow of a Carreau fluid during sphere impact," Phys. Fluids **24**, 073104 (2012).
[19]M. A. Rao, *Rheology of Fluid and Semisolid Foods: Principles and Applications* (Springer Science & Business Media, 2010).
[20]N. Rudolph and T. A. Osswald, *Polymer Rheology: Fundamentals and Applications* (Carl Hanser Verlag GmbH Co KG, 2014).
[21]A. Pantokratoras, "Steady flow of a non-Newtonian Carreau fluid across an unconfined circular cylinder," Meccanica **51**, 1007–1016 (2016).
[22]S. Shahsavari and G. H. McKinley, "Mobility of power-law and Carreau fluids through fibrous media," Phys. Rev. E **92**, 063012 (2015).